


Cite this: *RSC Adv.*, 2017, 7, 48785

# Facile preparation of high-performance Fe-doped Ce–Mn/TiO<sub>2</sub> catalysts for the low-temperature selective catalytic reduction of NO<sub>x</sub> with NH<sub>3</sub>†

Quan Xu, <sup>a</sup> Rigu Su,<sup>a</sup> Li Cao,<sup>a</sup> Yeqing Li,<sup>a</sup> Chuanyao Yang,<sup>b</sup> Yan Luo,<sup>c</sup> Jason Street,<sup>d</sup> Pengcheng Jiao<sup>e</sup> and Lulu Cai<sup>\*b</sup>

A Ce–Mn–Fe/TiO<sub>2</sub> catalyst has been successfully prepared using a single impregnation method, and excellent low-temperature NH<sub>3</sub>-SCR activity was demonstrated in comparison with other typical SCR catalysts including Mn–Ce/TiO<sub>2</sub> and metal-doped Mn–Ce/TiO<sub>2</sub>. The crystal structure, morphology, textural properties, valence state of the metals, acidity and redox properties of the novel catalyst were investigated comprehensively by X-ray diffraction (XRD), N<sub>2</sub> adsorption and desorption analysis, X-ray photoelectron spectroscopy (XPS), NH<sub>3</sub>-temperature-programmed desorption (NH<sub>3</sub>-TPD), and H<sub>2</sub>-temperature-programmed reduction (H<sub>2</sub>-TPR). The Fe-doped Ce–Mn/TiO<sub>2</sub> catalyst boosted the low-temperature NH<sub>3</sub>-SCR activity effectively under a broad temperature range (100–280 °C) with a superior NO conversion rate at low temperatures (100 °C, 96%; 120–160 °C, ~100%). Fe doping caused this improvement by enlarging the catalyst pore volume, improving the redox properties, and increasing the amount of acidic sites. These properties enhanced the ability of the catalyst to adsorb NH<sub>3</sub> and improved the low-temperature SCR performance, especially at temperatures lower than 150 °C. Moreover, redox cycles of Ce, Mn, and Ti (Mn<sup>4+</sup> + Ce<sup>3+</sup> ↔ Mn<sup>3+</sup> + Ce<sup>4+</sup>, Mn<sup>4+</sup> + Ti<sup>3+</sup> ↔ Mn<sup>3+</sup> + Ti<sup>4+</sup>) also played an important role in enhancing the low-temperature SCR efficiency by accelerating the electron transfer. The excellent NH<sub>3</sub>-SCR result is promising for developing environmentally-friendly and more effective industrial catalysts in the future.

Received 17th July 2017  
Accepted 13th October 2017

DOI: 10.1039/c7ra07854d

rsc.li/rsc-advances

## Introduction

Nitrogen oxides (NO, NO<sub>2</sub>, N<sub>2</sub>O) are mainly emitted from power plants and vehicles from the combustion of N-containing fossil fuels.<sup>1–3</sup> These nitrogen oxides cause severe pollution to the environment and negative human health effects.<sup>4–7</sup> Technology involving the selective catalytic reduction (SCR) of NO<sub>x</sub> with NH<sub>3</sub> (NH<sub>3</sub>-SCR) has grown in recognition as the most effective and the most widely used method.<sup>4,8,9</sup> SCR technology applied to upstream processes where ash arrangements are present (SO<sub>2</sub>, alkali metal ions, *etc.*) poison and deactivate catalysts quickly. In contrast, using catalysts after a desulfurization scrubber in

the presence of lower dust and sulfur concentrations has been shown to be a significantly superior method. This method increases the catalyst lifetime because a majority of the SO<sub>2</sub> and dust have been removed so that the deactivation of the catalyst does not readily take place.<sup>10</sup> The fundamental goal for downstream denitrification technology is to develop a SCR catalyst that possesses a high activity within lower-temperature ranges, possesses a strong anti-sulfur performance, and is vanadium-free to be environmentally friendly.

Metal oxide catalyst groups Mn-based<sup>11–15</sup> and Ce-based<sup>16–19</sup> have high efficiencies for low-temperature activity. The reduction of Mn<sup>4+</sup> to Mn<sup>3+</sup> in the Mn phase, and the large oxygen storage capacity and redox properties of CeO<sub>2</sub> cause this high efficiency. Smirniotis' group<sup>20,21</sup> applied the advanced instruments to full characterize the catalysts to reveal the mechanism of the NH<sub>3</sub>-SCR reaction in the presence of Mn-based catalysts. Moreover, previous studies have proven that the co-doped Mn–Ce catalysts<sup>22–25</sup> have better SCR activity at low-temperature ranges because of the synergistic effect between Ce, Mn, and their supports. Qi *et al.*<sup>26</sup> prepared a non-load-type MnO<sub>x</sub>–CeO<sub>2</sub>, low-temperature SCR catalyst using a co-precipitation method. The removal of NO was furthered by improving the ability of the redox catalyst to perform such that the Mn permeated the CeO<sub>2</sub> lattice, and this generated a large number of oxygen vacancies.

<sup>a</sup>State Key Laboratory of Heavy Oil Processing, Institute of New Energy, China University Petroleum, Beijing, 102249, China. E-mail: xuquan@cup.edu.cn

<sup>b</sup>Personalized Drug Therapy Key Laboratory of Sichuan Province, Hospital of the University of Electronic Science and Technology of China, Sichuan Provincial People's Hospital, Chengdu, Sichuan, 610072, P. R. China. E-mail: lzxulu@126.com

<sup>c</sup>Department of Chemical Engineering, West Virginia University, Morgantown, 26505, USA

<sup>d</sup>Department of Sustainable Bioproducts, Mississippi State University, 39762, USA

<sup>e</sup>Department of Civil and Environmental Engineering, Michigan State University, East Lansing, MI, 48824, USA

† Electronic supplementary information (ESI) available. See DOI: 10.1039/c7ra07854d



Lee *et al.*<sup>27</sup> prepared a MnO<sub>x</sub>/CeO<sub>2</sub>-TiO<sub>2</sub> catalyst, and Ce doping of this catalyst enhanced the catalytic activity by increasing the surface area of the catalyst while improving the Mn<sup>4+</sup> concentration. Shen *et al.*<sup>28</sup> prepared a Mn/Ce-ZrO<sub>2</sub> catalyst using an impregnation method, and NO conversion reached 98.6% at a temperature of 180 °C. Moreover, the Mn/Ce-ZrO<sub>2</sub> catalyst exhibited a resistance to water and sulfur with a NO conversion rate of 87% in the presence of 100 ppm SO<sub>2</sub> and 3% H<sub>2</sub>O. Liu *et al.*<sup>8</sup> proved that the environmentally benign Mn-Ce-Ti catalyst had a high affinity for NO<sub>x</sub> removal because of the dual redox properties and the amorphous structure of the catalyst. Moreover, the Mn-Ce-Ti catalyst displayed a high resistance toward H<sub>2</sub>O and SO<sub>2</sub>. The Co-doped Mn-Ce catalysts exhibited a high NO<sub>x</sub> removal efficiency and sulfur resistance in the SCR at a low-temperature range of 150–300 °C; however, NO<sub>x</sub> removal efficiency at temperatures lower than 150 °C still need to be improved to meet industry requirements.

The aim of this work is to further improve the low-temperature SCR co-doped Ce-Mn/TiO<sub>2</sub> catalyst activity by modifying the catalyst with Fe,<sup>19,29</sup> Cu<sup>17,30</sup> or Co.<sup>31</sup> A series of Ce-Mn-X/TiO<sub>2</sub> catalysts (where X = Fe, Cu, or Co) were prepared using a single impregnation method and investigated for the low-temperature SCR of NO<sub>x</sub> with NH<sub>3</sub>. The possible mechanism of the best performing low-temperature SCR catalyst in this work is discussed in detail using various characterization methods.

## Experimental section

### Materials

Cerium nitrate (100% purity), acetic acid manganese (100% purity), iron nitrate (100% purity), and copper nitrate (100% purity) were purchased from Sinopharm Chemical Reagent Co., Ltd. Nitric acid cobalt (100% purity) was purchased from the Tianjin Guangfu Technology Development. Nano TiO<sub>2</sub> was obtained from Tianjin Guangfu Fine Chemical Co., Ltd. Deionized water was prepared in the lab. All the chemicals were used without further purification.

### Catalyst preparation

The catalysts were prepared using a previously defined impregnation method.<sup>32</sup> First, 2.5 g of cerium nitrate, 1.46 g of acetic acid manganese and 2.15 g of iron nitrate (or 1.46 g copper nitrate or 1.55 g cobalt nitrate) were dissolved in deionized water, followed by stirring for 1 h to dissolve the solute completely. Five grams of nano TiO<sub>2</sub> was added to the solution and stirred for 2 h. Subsequently, water was removed using a rotary evaporation instrument at 60 °C. The remaining solid was dried at 105 °C in an oven for 24 h, and then calcined at 500 °C for 2 h in an air environment with a tube furnace at atmospheric conditions. The calcined samples were ground into a powder and sieved through a 20–40 mesh to perform catalytic activity evaluations. The mass ratios of Ce/TiO<sub>2</sub>, Mn/TiO<sub>2</sub> and X (Cu/Fe/Co)/TiO<sub>2</sub> catalysts were 0.2, 0.06, and 0.1, respectively.

### Catalyst activity measurement

SCR activity evaluation of all the catalysts were carried out in a fixed bed stainless steel tube reactor with an inner diameter of 11 mm and an outer diameter of 14 mm. Laboratory gas was purchased which contained specific concentrations of components to simulate flue gas in the experiment. The feed gas mixture consisted of 500 ppm NH<sub>3</sub>, 500 ppm NO, 3% O<sub>2</sub> (volume fraction), 100 ppm SO<sub>2</sub> and a balance of N<sub>2</sub>. The simulated gas flow rate was 1000 mL min<sup>-1</sup>. The nitrogen oxide concentrations were monitored in real-time by a gas analyzer (Testo 340). Six millilitres of each catalyst (20–40 mesh) was loaded for each reaction, and the experiment was performed between 100 and 300 °C at a heating rate of 3 °C min<sup>-1</sup> with a gas hourly space velocity (GHSV) of 10 000 h<sup>-1</sup>. The concentrations of NO were measured at the inlet and outlet with a flue gas analyzer to calculate the conversion rate using eqn (1). Eqn (1) describes the NO to NO<sub>2</sub> conversion.

$$\text{NO conversion (\%)} = \frac{[\text{NO}]_{\text{in}} - [\text{NO}]_{\text{out}}}{[\text{NO}]_{\text{in}}} \times 100\% \quad (1)$$

where [NO]<sub>in</sub> and [NO]<sub>out</sub> refer to the NO concentration at the reactor inlet [in] and outlet [out], respectively. The measurements were recorded in ppm. The concentration was measured when the reaction reached a steady state condition (about 20–40 min) at each temperature which reduced measurement errors caused by instability.

### Catalyst characterization

The powder X-ray diffraction (XRD) characterization of the samples was performed using a Bruker D8-Advance X-ray powder diffractometer with a Cu K $\alpha$  radiation source ( $\lambda = 1.5406 \text{ \AA}$ ), a pulverized sample with scattering angles ( $2\theta$ ) of 5–85°, and a 0.0197 step size operated at 50 kV and 50 mA. The diffraction lines were identified by matching them with reference patterns from the Joint Committee on Powder Diffraction Standards (JCPDS) database.

A ThermoFisher Escalab 250Xi X-ray powder photoelectron spectrometer was used to qualitatively analyze the X-ray photoelectron spectroscopy (XPS) characterization of the sample surface composition using an Al K $\alpha$  radiation source with a scattering of 0–5000 eV. The binding energy was calibrated using the C 1s peak contaminate carbon (BE = 284.6 eV) as an internal standard.

N<sub>2</sub> adsorption and desorption of each sample was measured at –196 °C using the ASAP 2020 automatic rapid surface area and mesopore/microporous analyzer with a N<sub>2</sub> adsorption gas. The samples were degassed at 200 °C for 12 h before the analysis occurred. The specific surface area was calculated according to the Brunauer–Emmett–Teller (BET) method. The total pore volume was determined based on the amount of the adsorbed N<sub>2</sub> volume at a relative pressure of approximately  $p/p^0 = 0.99$ .

Temperature programmed reduction with H<sub>2</sub> (H<sub>2</sub>-TPR) was performed using a MICROMERITICS Autochem 2920 fully automatic chemistry-adsorption-tester. A sample with a mass of 0.1 g was pretreated under a He atmosphere with a heating rate



of  $10\text{ }^{\circ}\text{C min}^{-1}$  until reaching at  $300\text{ }^{\circ}\text{C}$  and then cooled to  $40\text{ }^{\circ}\text{C}$ . Subsequently,  $10\%\text{ H}_2\text{-Ar}$  flowed through the catalyst bed while the temperature was ramped from  $40\text{ }^{\circ}\text{C}$  to  $900\text{ }^{\circ}\text{C}$  at a heating rate of  $10\text{ }^{\circ}\text{C min}^{-1}$ . The hydrogen consumption signal was measured by a thermal conductivity detector (TCD).

Temperature programmed desorption of ammonia ( $\text{NH}_3$ -TPD) was performed using a MICROMERITICS Autochem 2920 fully automatic chemistry-adsorption-tester. A sample with a mass of  $0.1\text{ g}$  was pretreated under a He atmosphere at  $600\text{ }^{\circ}\text{C}$  for  $1\text{ h}$  and then saturated with high purity ammonia at  $40\text{ }^{\circ}\text{C}$  for  $1\text{ h}$ . Subsequently, helium was flowed through the sample at the same temperature for  $1\text{ h}$  to remove ammonia. TCD desorption was performed from  $100$  to  $500\text{ }^{\circ}\text{C}$  at a heating rate of  $10\text{ }^{\circ}\text{C min}^{-1}$ , and the ammonia was detected by the TCD.

## Results and discussion

### $\text{NH}_3$ -SCR performance at low-temperatures

The  $\text{NH}_3$ -SCR activities of  $\text{Ce/TiO}_2$ ,  $\text{Mn/TiO}_2$ , co-doped  $\text{Ce-Mn/TiO}_2$ , and X (Fe, Co, Cu) modified  $\text{Ce-Mn/TiO}_2$  catalyst were determined between  $100$  and  $300\text{ }^{\circ}\text{C}$ , and the results are shown in Fig. 1. Both  $\text{Ce/TiO}_2$  and  $\text{Mn/TiO}_2$  have a certain low-temperature  $\text{NH}_3$ -SCR activity, while  $\text{Mn/TiO}_2$  showed a higher NO conversion than  $\text{Ce/TiO}_2$  below  $200\text{ }^{\circ}\text{C}$ . However, the NO conversion was lower than  $40\%$  in the presence of the  $\text{Ce/TiO}_2$  and  $\text{Mn/TiO}_2$  catalysts. In contrast, co-doped  $\text{Ce-Mn/TiO}_2$  catalysts afforded highly remarkable catalytic activity. The co-doped catalysts demonstrated catalytic activity under a wide temperature operation window. A NO conversion of  $90\%$  was obtained from  $140$  to  $280\text{ }^{\circ}\text{C}$ , and nearly  $100\%$  NO conversion was obtained at  $160\text{ }^{\circ}\text{C}$ . This improvement has also been demonstrated in another study;<sup>8</sup> however, high  $\text{NH}_3$ -SCR activities at low-temperature have not been determined in the co-doped  $\text{Ce-Mn/TiO}_2$  catalysts.

To enhance  $\text{NH}_3$ -SCR activities below  $150\text{ }^{\circ}\text{C}$ , the  $\text{Ce-Mn/TiO}_2$  catalyst was modified using Fe, Co or Cu. Fe addition has

been demonstrated to greatly improve  $\text{NH}_3$ -SCR activity with a conversion of  $96.8\%$  at  $180\text{ }^{\circ}\text{C}$  in the presence of  $\text{Fe-Ce-Mn/TiO}_2$  catalysts prepared *via* a sol-gel method.<sup>19</sup> In this study, the Fe-doped,  $\text{Ce-Mn/TiO}_2$  catalyst prepared by an impregnation method improved the low-temperature  $\text{NH}_3$ -SCR by increasing the NO conversion from  $43.2\%$  to  $96.3\%$  at  $100\text{ }^{\circ}\text{C}$ . The NO conversion below  $200\text{ }^{\circ}\text{C}$  was improved to greater than  $90\%$  within the temperature range  $100\text{--}260\text{ }^{\circ}\text{C}$ . Nearly  $100\%$  NO conversion occurred between  $120\text{--}160\text{ }^{\circ}\text{C}$ , indicating  $\text{Fe-Ce-Mn/TiO}_2$  was very active and selective for  $\text{NH}_3$ -SCR of NO at temperatures lower than  $150\text{ }^{\circ}\text{C}$ . This catalyst was shown to have the highest NO conversion concerning the SCR reaction at temperatures lower than  $150\text{ }^{\circ}\text{C}$  when compared to other studies thus far. The catalyst preparation approach played a vital role in  $\text{NH}_3$ -SCR process efficiency. However, the Co-doped catalyst had a minuscule impact on the  $\text{Ce-Mn/TiO}_2$  catalytic performance, and the Cu-doped catalyst had a substantially negative effect on the low-temperature activity; the NO conversion was reduced from  $43.2\%$  to  $13.6\%$  at  $100\text{ }^{\circ}\text{C}$  after using Cu to dope the catalyst. The comparisons of the  $\text{NH}_3$ -SCR activities with the reported results in recent studies are summarized in Table S1.† The  $\text{Fe-Ce-Mn/TiO}_2$  catalyst was the only catalyst selected for further study and characterization because of the excellent  $\text{NH}_3$ -SCR activity at temperatures below  $150\text{ }^{\circ}\text{C}$ .

### Effect of Fe doped $\text{Ce-Mn/TiO}_2$ catalysts on NO oxidation

The effects of Ce, Mn and Fe doped  $\text{TiO}_2$  catalysts on NO oxidation were investigated under the conditions of  $500\text{ ppm NO}$  and  $3\%\text{ O}_2$  at a temperature range of  $100\text{--}300\text{ }^{\circ}\text{C}$ . The results in Fig. 2 show that NO oxidation rates in the presence of  $\text{Ce/TiO}_2$  and  $\text{Mn/TiO}_2$  catalysts were below  $35\%$  at  $100\text{--}300\text{ }^{\circ}\text{C}$ . Co-doping Ce and Mn improved the NO oxidation at higher temperatures ranging from  $160$  to  $300\text{ }^{\circ}\text{C}$ . The oxidation rate reached approximately  $80\%$  at  $300\text{ }^{\circ}\text{C}$ . The NO oxidation rate in the presence of Fe modified  $\text{Ce-Mn/TiO}_2$  catalysts was much higher than the single  $\text{Ce/TiO}_2$  or  $\text{Mn/TiO}_2$  catalyst. The NO

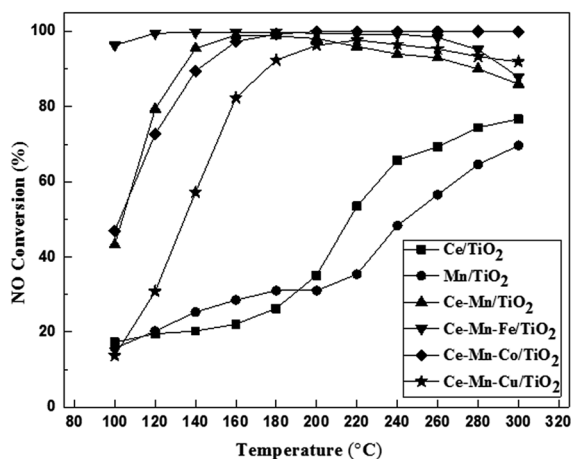


Fig. 1  $\text{NH}_3$ -SCR activity of  $\text{Ce/TiO}_2$ ,  $\text{Mn/TiO}_2$ , co-doped  $\text{Ce-Mn/TiO}_2$  and X (Fe, Co, Cu) modified  $\text{Ce-Mn/TiO}_2$  catalysts (experimental conditions:  $500\text{ ppm NO}$ ,  $500\text{ ppm NH}_3$ ,  $3\%\text{ O}_2$ ,  $\text{N}_2$  balance gas,  $\text{GHSV} = 10\,000\text{ h}^{-1}$ ).

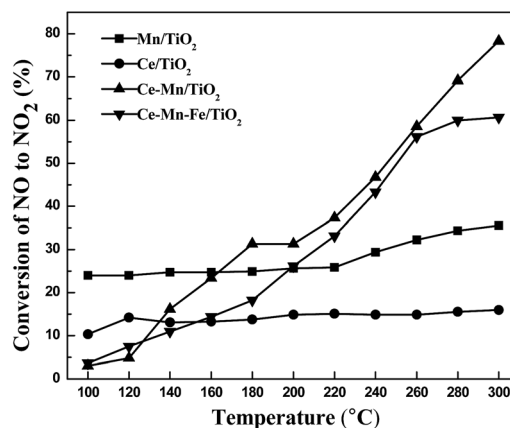


Fig. 2 Effect of Fe doped  $\text{Ce-Mn/TiO}_2$  catalysts on the NO oxidation (experimental conditions:  $500\text{ ppm NO}$ ,  $3\%\text{ O}_2$ ,  $\text{N}_2$  balance gas,  $\text{GHSV} = 10\,000\text{ h}^{-1}$ ).



oxidation rate of the Fe modified catalysts was only slightly reduced when compared with the Ce–Mn/TiO<sub>2</sub> catalyst at higher temperatures of 200–280 °C.

The Fe modified Ce–Mn/TiO<sub>2</sub> catalysts reduced the oxidation properties of NO to NO<sub>2</sub> when compared to non-Fe modified catalysts. Moreover, Fe modified Ce–Mn/TiO<sub>2</sub> catalysts showed a much lower NO oxidation level at low temperatures than the single Mn/TiO<sub>2</sub> catalyst. Currently, most studies suggest that rapid SCR reactions ( $2\text{NH}_3 + \text{NO} + \text{NO}_2 \rightarrow 2\text{N}_2 + 3\text{H}_2\text{O}$ ) with faster reaction rates occur at low temperatures when using Ce and Mn doped catalysts due to their superior low-temperature denitrification properties.<sup>33</sup> This study has shown that Ce–Mn/TiO<sub>2</sub> and Ce–Mn–Fe/TiO<sub>2</sub> catalysts improved the NO oxidation reaction to produce NO<sub>2</sub> which would promote a rapid SCR reaction at high temperatures above 200 °C while decreasing the NO oxidation rate at temperatures less than 200 °C. Therefore, the high NH<sub>3</sub>-SCR activity of the Ce–Mn–Fe/TiO<sub>2</sub> catalyst (96% NO conversion at 100 °C and nearly 100% between 120–160 °C) was not realized by enhancing the NO oxidation.

### Resistance to SO<sub>2</sub> poisoning on Fe doped Ce–Mn/TiO<sub>2</sub> catalysts

The effect of SO<sub>2</sub> on the SCR activity of Ce–Mn/TiO<sub>2</sub> and Ce–Mn–Fe/TiO<sub>2</sub> catalysts was investigated at a temperature of 160 °C, and the results are shown in Fig. 3.

In the absence of SO<sub>2</sub>, both Ce–Mn/TiO<sub>2</sub> and Ce–Mn–Fe/TiO<sub>2</sub> catalysts had excellent stability for 7 h, and the NO conversion was approximately 100%. After adding 100 ppm of SO<sub>2</sub>, the SCR activity of Ce–Mn/TiO<sub>2</sub> decreased rapidly to a NO conversion of 83% in 50 min. This NO conversion remained constant at 80% throughout the test. After the SO<sub>2</sub> was removed from the stream, the SCR activity increased to approximately 92%, but it did not recover completely. After 100 ppm of SO<sub>2</sub> was added to the stream, the NO conversion of the Ce–Mn–Fe/TiO<sub>2</sub> catalyst decreased to 40% after 5 h. After the SO<sub>2</sub> was removed from the stream, the SCR activity continued to decline with no recovery for another 1 h. After the catalyst was doped with Fe, the sulfur

resistance performance severely decreased. The loss of catalyst activity was possibly due to competing reactant adsorption mechanisms occurring on the catalyst surface.<sup>10</sup> Furthermore, the active component Fe<sub>2</sub>O<sub>3</sub> of the catalyst easily reacts with SO<sub>2</sub> and O<sub>2</sub> to produce the component Fe<sub>2</sub>(SO<sub>4</sub>)<sub>3</sub> which leads to poisoning and deactivation of catalysts.<sup>24</sup>

### Resistance to H<sub>2</sub>O poisoning on Fe doped Ce–Mn/TiO<sub>2</sub> catalysts

At low temperatures, water vapor (H<sub>2</sub>O) in the flue gas is a key factor that can lead to the deactivation of a SCR catalyst. The resistance of the catalyst under these H<sub>2</sub>O conditions at low temperatures was investigated. Fig. 4 shows the comparison of NO conversion using Ce–Mn/TiO<sub>2</sub> and Ce–Mn–Fe/TiO<sub>2</sub> catalysts in the presence of 1 vol% H<sub>2</sub>O. Before the addition of H<sub>2</sub>O, the SCR reaction was stabilized at 200 °C for 3 h, and the NO conversion was 91.9% and 97.3% in the presence of the Ce–Mn/TiO<sub>2</sub> and Ce–Mn–Fe/TiO<sub>2</sub> catalysts, respectively. When 1 vol% of H<sub>2</sub>O was added into the flue gas, the NO conversion immediately decreased to 76.3% and 81.5% for the Ce–Mn/TiO<sub>2</sub> and the Ce–Mn–Fe/TiO<sub>2</sub> catalysts in 6 h, respectively. After undergoing 6 h in the presence of 1 vol% H<sub>2</sub>O, the H<sub>2</sub>O was removed from the flue gas, and after 4 h the NO conversion was 78.5% and 80.4% for the Ce–Mn/TiO<sub>2</sub> and Ce–Mn–Fe/TiO<sub>2</sub> catalysts, respectively. The H<sub>2</sub>O exhibited a largely irreversible effect on the activities of these catalysts. The presence of water vapor in the flue gas inhibited the reactant adsorption over the catalyst surface, and the reduced adsorption of the reactant was found to have an irreversible effect on the activity of the catalysts. However, the addition of Fe improved the resistance of H<sub>2</sub>O poisoning on Ce–Mn/TiO<sub>2</sub> catalyst.

### Catalyst characterization

X-ray powder diffraction patterns of different catalysts are shown in Fig. 5. The diffraction peaks of anatase titanium dioxide were observed in all four catalysts, and no diffraction

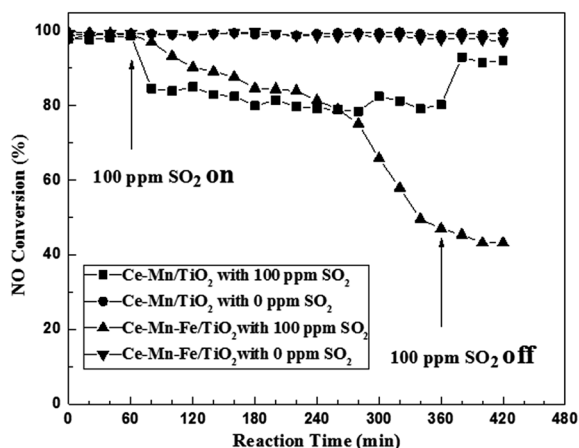


Fig. 3 Resistance to SO<sub>2</sub> poisoning on Fe doped Ce–Mn/TiO<sub>2</sub> catalysts (experimental conditions: 500 ppm NO, 500 ppm NH<sub>3</sub>, 3% O<sub>2</sub>, N<sub>2</sub> balance gas, 0 or 100 ppm SO<sub>2</sub>, GHSV = 10 000 h<sup>−1</sup>).

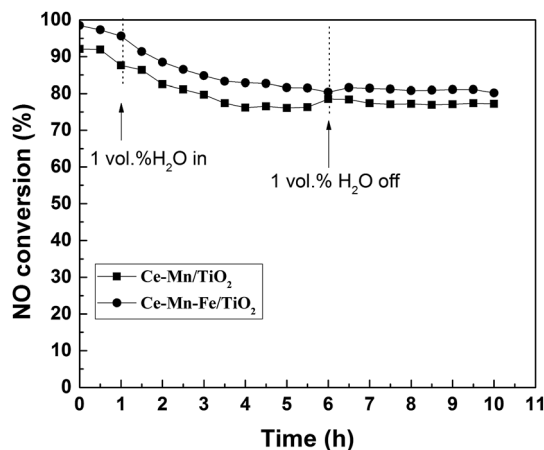


Fig. 4 Resistance to H<sub>2</sub>O poisoning on Fe doped Ce–Mn/TiO<sub>2</sub> catalysts (experimental conditions: 500 ppm NO, 500 ppm NH<sub>3</sub>, 3% O<sub>2</sub>, N<sub>2</sub> balance gas, 0 or 1 vol% H<sub>2</sub>O, GHSV = 10 000 h<sup>−1</sup>).





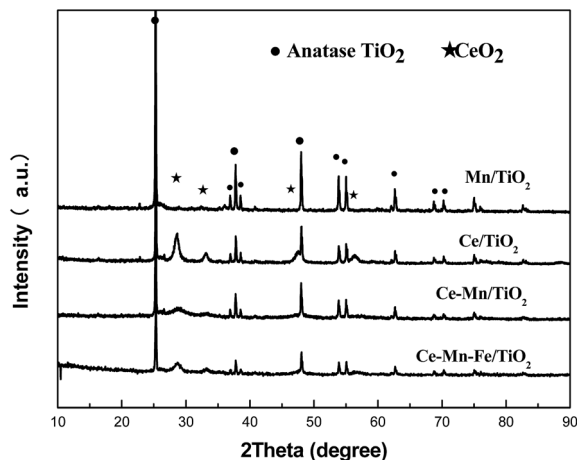


Fig. 5 XRD profiles of different catalysts.

peaks of the brookite and rutile phases were observed. The diffraction peak of manganese oxide was not observed. This observation suggests the distribution of manganese oxides on the catalyst surface was uniform, and no large  $\text{MnO}_x$  grains were produced. The XRD pattern of  $\text{Ce}/\text{TiO}_2$  showed sharp diffraction peaks of  $\text{CeO}_2$  at  $2\theta = (28.6^\circ, 33.1^\circ, 47.6^\circ \text{ and } 56.5^\circ)$ . XRD patterns of the  $\text{Ce-Mn}/\text{TiO}_2$  catalyst showed a diffraction peak of  $\text{CeO}_2$  at  $2\theta = 28.6^\circ$ , and a lower peak intensity than that of the  $\text{Ce}/\text{TiO}_2$  catalyst. This indicated that Ce and Mn doping can promote the dispersion of  $\text{CeO}_2$  on the catalyst surface and reduce the degree of crystallization. The diffraction peaks of  $\text{CeO}_2$  and  $\text{TiO}_2$  were similar to the  $\text{Ce-Mn}/\text{TiO}_2$  catalyst, and no  $\text{FeO}_x$  peak was observed in the XRD pattern of the  $\text{Ce-Mn-Fe}/\text{TiO}_2$  catalyst. This indicated that Fe possibly existed in an amorphous or highly dispersed phase on the surface of the catalyst. After Fe doping, the active components of the catalyst remained well dispersed. This is also one of the reasons for the excellent catalytic activity of  $\text{Ce-Mn-Fe}/\text{TiO}_2$  at low temperatures.<sup>24</sup> SEM images of the  $\text{Ce-Mn-Fe}/\text{TiO}_2$  catalyst were captured at four scales (500 nm, 1.0  $\mu\text{m}$ , 2.0  $\mu\text{m}$  and 5  $\mu\text{m}$ ) and

are shown in Fig. 6(a–d). These images clearly confirmed that the Mn–Ce–Fe metal oxides were highly dispersed on the catalyst surface. The images also prove that the catalyst had homogenous particle sizes and shapes.

Table 1 shows the effects of Ce, Mn, and Fe doping on the BET surface area and pore structure of the catalysts investigated with  $\text{N}_2$  adsorption–desorption experiments. After Ce and Mn co-doping, the specific surface area and pore volume of the  $\text{Ce-Mn}/\text{TiO}_2$  catalyst increased substantially more than the  $\text{Ce}/\text{TiO}_2$  and  $\text{Mn}/\text{TiO}_2$  catalysts. Fe doping on the  $\text{Ce-Mn}/\text{TiO}_2$  catalyst enlarged the specific surface area, the pore volume, and pore size. This improvement is possibly due to the synergy of the Mn and Fe, which facilitated the dispersion of the active components on the catalyst and improved the low temperature activity.<sup>24,34</sup>

Fig. 7 shows the effect of Fe doping on the redox properties of the catalysts investigated by hydrogen temperature-programmed reduction ( $\text{H}_2$ -TPR) experiments. The hydrogen reduction peak at  $T_1$  (352  $^\circ\text{C}$ ) and  $T_2$  (435  $^\circ\text{C}$ ) were attributed to the transformation of  $\text{MnO}_2 \rightarrow \text{Mn}_2\text{O}_3$  and  $\text{Mn}_2\text{O}_3 \rightarrow \text{Mn}_3\text{O}_4$ , respectively.<sup>41</sup> The hydrogen reduction peaks at  $T_3$  (596  $^\circ\text{C}$ ) and  $T_4$  (726  $^\circ\text{C}$ ) were attributed to transformations of surface  $\text{CeO}_2 \rightarrow \text{Ce}_2\text{O}_3$  and crystal lattice  $\text{CeO}_2 \rightarrow \text{Ce}_2\text{O}_3$ , respectively.<sup>35</sup> After the catalyst was doped with Fe, the reduction peak area of hydrogen increased significantly, indicating that Fe doping increased the oxidation–reduction capacity of the catalyst. Moreover, the reduction temperature of the crystal lattice transformation of  $\text{CeO}_2 \rightarrow \text{Ce}_2\text{O}_3$  was decreased. This indicated that the ceria oxide became more reducible, and can be ascribed to the synergetic effect between Ce and Fe.  $\text{NH}_3$ -SCR reactions consume active oxygen on the catalyst surface and undergo several redox reactions.<sup>24</sup> This may be another reason for the high  $\text{NH}_3$ -SCR activity of  $\text{Ce-Mn-Fe}/\text{TiO}_2$  at low temperatures.

Fig. 8 shows the effect of Fe doping on the surface acidity of  $\text{Ce-Mn}/\text{TiO}_2$  catalysts using ammonia temperature-programmed desorption ( $\text{NH}_3$ -TPD). The  $\text{NH}_3$  desorption peak in the temperature range of 80–200  $^\circ\text{C}$  was caused by desorption of  $\text{NH}_3$  at the weak acidic sites. The  $\text{NH}_3$  desorption peak at 200–350  $^\circ\text{C}$  was due to desorption of  $\text{NH}_3$  on the medium strength acidic sites. The  $\text{Ce-Mn}/\text{TiO}_2$  catalyst only had weak acid sites, while the  $\text{Ce-Mn-Fe}/\text{TiO}_2$  catalyst had both weak and medium strength acidic sites.<sup>27</sup> The adsorption of  $\text{NH}_3$  on the catalyst surface was a key step in the SCR reaction, regardless of the reaction in the Langmuir–H or Eideall–Rley pathway.<sup>27,36,37</sup> Fe doping not only increased the number of weak acidic sites on the catalyst but also produced medium acidic sites. The enhancement of the surface acidity of the catalyst contributed to the adsorption and activation of  $\text{NH}_3$ . This was an important

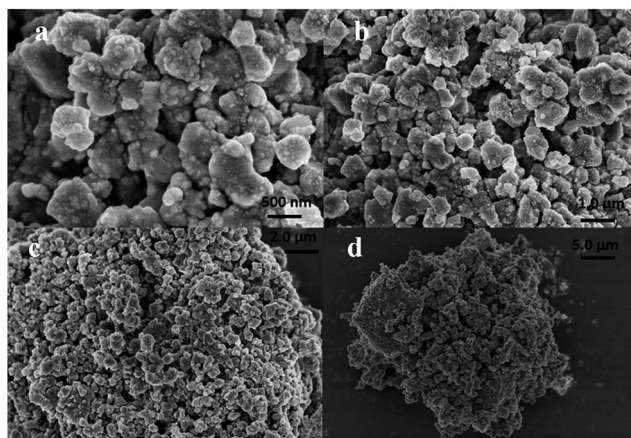


Fig. 6 SEM images of the Mn–Ce–Fe/ $\text{TiO}_2$  catalyst. (a) 500 nm, (b) 1.0  $\mu\text{m}$ , (c) 2.0  $\mu\text{m}$  and (d) 5  $\mu\text{m}$ .

Table 1  $\text{N}_2$  adsorption and desorption results

Catalyst	$S_{\text{BET}}/\text{m}^2 \text{ g}^{-1}$	$V_p/\text{cm}^3 \text{ g}^{-1}$	$D/\text{nm}$
Mn/ $\text{TiO}_2$	10.17	0.0448	17.64
Ce/ $\text{TiO}_2$	14.21	0.0654	18.4
Ce-Mn/ $\text{TiO}_2$	28.81	0.0699	9.707
Ce-Mn-Fe/ $\text{TiO}_2$	30.41	0.1022	13.45



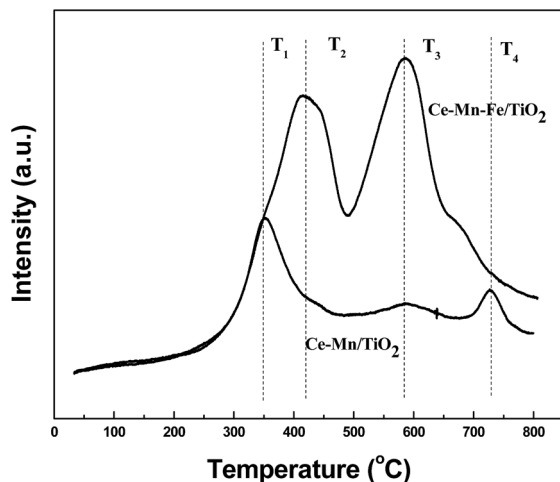


Fig. 7  $\text{H}_2$ -TPR profiles of Ce-Mn/TiO<sub>2</sub> and Ce-Mn-Fe/TiO<sub>2</sub> catalysts.

reason for the low temperature activity of Ce-Mn-Fe/TiO<sub>2</sub> catalysts.<sup>24</sup> This is especially applicable to the increased quantity of the weak acidic sites, where unstable or metastable nitrates species were produced at low-temperatures. These species did not occupy the active sites for extended periods of time and therefore improved the low-temperature SCR performance.<sup>17</sup>

The XPS spectra of the Ce, Mn, Ti, Fe, and O of the Ce-Mn/TiO<sub>2</sub> and Ce-Mn-Fe/TiO<sub>2</sub> catalysts are shown in Fig. 9(a–e). XPS spectra of Ce 3d of the Ce-Mn/TiO<sub>2</sub> and Ce-Mn-Fe/TiO<sub>2</sub> catalyst are shown in Fig. 9(a). The spectrum of Ce 3d contained eight peaks, six of which are the characteristic peaks of Ce<sup>4+</sup> and two of which are the characteristic peaks of Ce<sup>3+</sup>. The relative surface concentration of the element valence was calculated by the peak area shown in Table 2. The ratio of Ce<sup>3+</sup>/Ce<sup>4+</sup> decreased from 15.9% to 12.8% when comparing the Fe-doped catalyst to the Ce-Mn/TiO<sub>2</sub> catalyst. Cerium oxide can undergo the process of oxygen storage and oxygen release by the valence state's transformation of the electron pair (Ce<sup>3+</sup>/Ce<sup>4+</sup>) and improve the ability of the catalyst to convert NO to NO<sub>2</sub> (improving low-temperature activity).

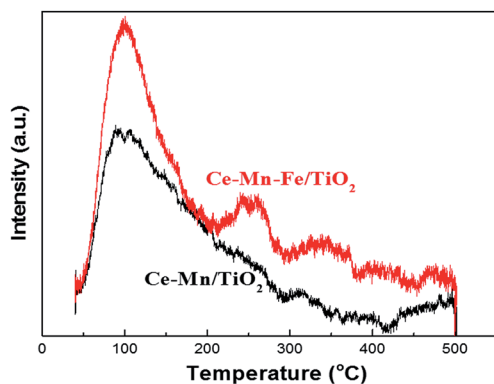


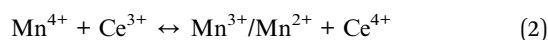
Fig. 8  $\text{NH}_3$ -TPD profiles of Ce-Mn/TiO<sub>2</sub> and Ce-Mn-Fe/TiO<sub>2</sub> catalysts.

The XPS spectra of Mn 2p of the Ce-Mn/TiO<sub>2</sub> and Ce-Mn-Fe/TiO<sub>2</sub> catalysts are shown in Fig. 9(b). The spectrum of Mn 2p contains the characteristic peaks of Mn<sup>2+</sup>, Mn<sup>3+</sup>, and Mn<sup>4+</sup>.<sup>38</sup> The relative surface concentration of the element valence was calculated using the peak area shown in Table 2. The ratio of Mn<sup>4+</sup>/Mn<sup>3+</sup> increased from 84.0% to 86.2% after Fe was doped onto the Ce-Mn/TiO<sub>2</sub> catalyst. The catalytic effect of MnO<sub>x</sub> was related to its valence state, where MnO<sub>2</sub> > Mn<sub>2</sub>O<sub>3</sub> > MnO,<sup>30</sup> this has also been demonstrated by Boningari *et al.*<sup>39</sup> indicating that MnO<sub>2</sub> was the most active among a series comprising MnO<sub>2</sub>, Mn<sub>5</sub>O<sub>8</sub>, Mn<sub>2</sub>O<sub>3</sub> and Mn<sub>3</sub>O<sub>4</sub>.

The XPS spectra of Ti 2p of the Ce-Mn/TiO<sub>2</sub> and Ce-Mn-Fe/TiO<sub>2</sub> catalysts are shown in Fig. 9(c). The spectrum peaks of Ti 2p<sub>3/2</sub> and Ti 2p<sub>1/2</sub> at the binding energy of 458.6 eV and 464.3 eV, respectively, are attributable to the characteristic peak of Ti<sup>3+</sup> and Ti<sup>4+</sup>.<sup>40</sup> Compared to Ce-Mn/TiO<sub>2</sub> catalyst, the Ti 2p peak position of the Ce-Mn-Fe/TiO<sub>2</sub> catalyst was shifted to the right by approximately 0.3 eV, indicating some of the Ti<sup>4+</sup> ions were reduced to Ti<sup>3+</sup> ions. The Ti<sup>3+</sup>/Ti<sup>4+</sup> ratio increased from 36.8% to 49.6% after the addition of Fe as shown in Table 2. The high reducibility of Ti contributes to the improvement of the NH<sub>3</sub>-SCR efficiency. The redox cycle of Ti<sup>4+</sup>/Ti<sup>3+</sup> is hypothesized to be another reason for the high SCR performance at low-temperature conditions.

The XPS spectra of Fe 2p of the Ce-Mn/TiO<sub>2</sub> and Ce-Mn-Fe/TiO<sub>2</sub> catalysts are shown in Fig. 9(d). The spectrum peaks of Fe 2p<sub>3/2</sub> and Fe 2p<sub>1/2</sub> are at the binding energy of 710.4 eV and 724.0 eV respectively, which are mainly assigned to Fe<sup>3+</sup>.<sup>14</sup> However, the Fe 2p<sub>3/2</sub> peak is obviously an asymmetrical distribution and the peak is broad, indicating the existence of Fe<sup>2+</sup>. Moreover, compared to the standard spectrum of Fe, the binding energy of Fe 2p<sub>3/2</sub> was shifted to a higher energy. This is because of the strong interaction between Fe and Mn or Ce led to the change of the electron cloud of Fe. The ratio of Fe<sup>2+</sup>/Fe<sup>3+</sup> was 8.28 as shown in Table 2. The Fe element mainly existed in the form of Fe<sup>3+</sup> in the catalyst, which can be reduced to Fe<sup>2+</sup>. The Fe redox cycles Fe<sup>3+</sup>/Fe<sup>2+</sup> is hypothesized to be another reason for the high SCR performance at low-temperature conditions.

The XPS spectra of O 1s of the Ce-Mn/TiO<sub>2</sub> and Ce-Mn-Fe/TiO<sub>2</sub> catalysts are shown in Fig. 9(e). The spectrum of O 1s contains characteristic peaks of O<sub>T</sub> and O<sub>b</sub>, where O<sub>T</sub> belongs to the characteristic peak of lattice oxygen at a binding energy of 529.5–529.8 eV, and O<sub>b</sub> belongs to the surface adsorption characteristic peaks of oxygen at a binding energy of 531.8–532.5 eV.<sup>14</sup> The relative surface concentration of the element valence calculated by the peak area is shown in Table 2. The surface adsorption of the oxygen concentration on the Ce-Mn/TiO<sub>2</sub> catalyst was 43.6% and remained unchanged after Fe was doped onto the Ce-Mn/TiO<sub>2</sub> catalyst. The high concentration of the surface adsorption oxygen had a strong oxidation effect, which not only completed the oxidation and reduction cycle<sup>8,24</sup> but also enhanced the oxidation process of NO to NO<sub>2</sub>. This promoted a rapid response to the SCR reaction.<sup>41</sup>



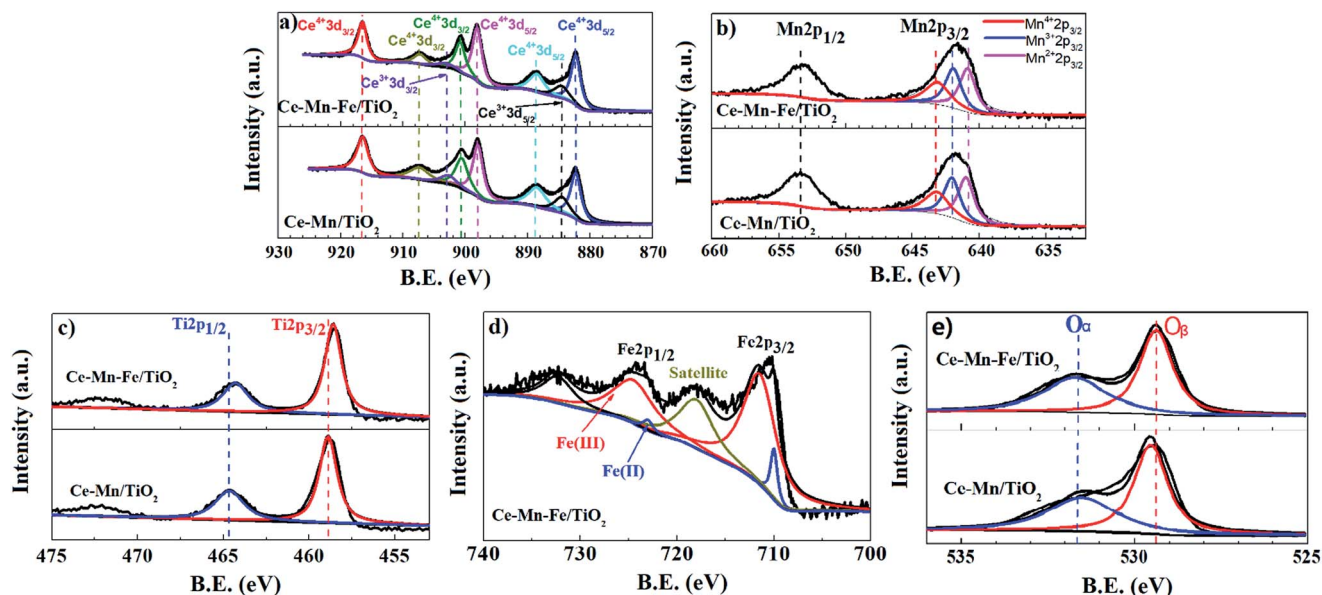
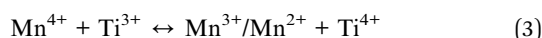


Fig. 9 XPS spectra of elements of catalysts. (a) Ce 3d, (b) Mn 2p, (c) Ti 2p, (d) Fe 2p, and (e) O 1s.

Table 2 Surface valence state ratios of Ce 3d, Mn 2p, Ti 2p, Fe 2p and O 1s of the catalysts

Catalyst	Surface element valence state (%)				
	Ce <sup>3+</sup> /Ce <sup>4+</sup>	Mn <sup>4+</sup> /Mn <sup>3+</sup>	Ti <sup>3+</sup> /Ti <sup>4+</sup>	O <sub>b</sub> /O <sub>T</sub>	Fe <sup>2</sup> /Fe <sup>3+</sup>
Ce-Mn/TiO <sub>2</sub>	15.9	84.0	36.8	43.6	
Ce-Mn-Fe/TiO <sub>2</sub>	12.8	86.2	49.6	43.5	8.28



In summary, the Fe-doped Ce-Mn/TiO<sub>2</sub> catalyst increased the number of weak and medium strength acidic sites, and properties of the catalyst were analyzed using XRD, BET, XPS, H<sub>2</sub>-TPR, and NH<sub>3</sub>-TPD. Doping the catalyst with Fe also increased the surface area, which increased NH<sub>3</sub> adsorption on the catalyst to boost the low-temperature SCR activity. Moreover, the addition of Fe enhanced the redox properties of the catalyst which accelerated the electron transfer.<sup>8,17</sup> Based on the XPS analysis results, the high ratios of Mn<sup>4+</sup>/Mn<sup>3+</sup> or Mn<sup>2+</sup>, Ce<sup>4+</sup>/Ce<sup>3+</sup>, and Ti<sup>4+</sup>/Ti<sup>3+</sup> could form dual redox cycles as shown in eqn (2) and (3), which accelerated the electron transfer and improved the NH<sub>3</sub>-SCR performance.<sup>8</sup>

## Conclusions

The modification of Ce-Mn/TiO<sub>2</sub> catalysts by doping Fe, Cu, or Co revealed that Cu doping significantly decreased the low-temperature NH<sub>3</sub>-SCR activity. Co doping had little obvious effect on NH<sub>3</sub>-SCR low-temperature activity. Fe doping effectively improved the low-temperature NH<sub>3</sub>-SCR activity. The NO conversion rate in the presence of the Ce-Mn-Fe/TiO<sub>2</sub> catalyst achieved 96% at the low temperature of 100 °C. The NO conversion was maintained at 90% between 100 and 280 °C. Fe doping also reduced the sulfur-poisoning resistance for SCR. In

the presence of 100 ppm SO<sub>2</sub>, the catalytic activity continued to decline and the NO conversion dropped to approximately 40% after 5 h at 160 °C. The SO<sub>2</sub> poisoning was the main reason for the decrease in catalytic activity. XRD, BET, H<sub>2</sub>-TPR, NH<sub>3</sub>-TPD and XPS characterization results demonstrated that Fe<sub>2</sub>O<sub>3</sub> was dispersed and well-proportioned on the surface of the catalyst. Fe-doping Ce-Mn/TiO<sub>2</sub> catalysts increased the specific surface area, enhanced the redox performance, and increased the surface acidity, especially to the medium strength acidic sites. Fe-doping had little impact on the valence states of other elements on the surface which still maintained a high proportion of Ce<sup>4+</sup>/Ce<sup>3+</sup>, Mn<sup>4+</sup>/Mn<sup>3+</sup>, Ti<sup>4+</sup>/Ti<sup>3+</sup> and O<sub>b</sub>/O<sub>T</sub>, respectively. The redox cycles between Mn, Ce, Fe, and Ti were one reason for the excellent low-temperature NH<sub>3</sub>-SCR efficiency. In summary, Fe-doped Ce-Mn/TiO<sub>2</sub> catalysts were observed to be environmentally friendly, effective, and an attractive catalyst for low-temperature SCR, especially at temperature ranges of less than 150 °C.

## Conflicts of interest

The authors declare no competing financial interest.

## Acknowledgements

We would like to thank the Beijing Nova Program (No. Z171100001117058), Beijing Municipal Science and Technology Project (No. Z161100001316010, D141100002814001), National Key Research and Development Plan (No. 2016YFC0303701) and the Science Foundation of China University of Petroleum-Beijing (No. C201604, 2462014YJRC) for the support. This material is also supported by the National Institute of Food and Agriculture, U.S. Department of Agriculture, and McIntire Stennis under accession number 1009735.





## Notes and references

- 1 T. Boningari and P. G. Smirniotis, *Curr. Opin. Chem. Eng.*, 2016, **13**, 133–141.
- 2 C. Yu, B. Huang, L. Dong, F. Chen and X. Liu, *Catal. Today*, 2017, **281**, 610–620.
- 3 K. Yang, W. Xiao, Q. Xu, J. Bai, Y. Luo, H. Guo, L. Cao, W. Cai, P. Pu and L. Cai, *J. Nanomater.*, 2017, 7901686.
- 4 W. Zhu, S. Xiao, D. Zhang, P. Liu, H. Zhou, W. Dai, F. Liu and H. Li, *Langmuir*, 2015, **31**, 10822–10830.
- 5 Z. Liu, J. Zhu, J. Li, L. Ma and S. I. Woo, *ACS Appl. Mater. Interfaces*, 2014, **6**, 14500–14508.
- 6 Y. Luo, V. K. Guda, P. H. Steele, B. Mitchell and F. Yu, *Energy Convers. Manage.*, 2016, **112**, 319–327.
- 7 Y. Luo, V. Guda, R. Wijayapala and P. H. Steele, *Energy Convers. Manage.*, 2016, **115**, 159–166.
- 8 Z. Liu, J. Zhu, J. Li, L. Ma and S. I. Woo, *ACS Appl. Mater. Interfaces*, 2014, **6**, 14500–14508.
- 9 Z. Liu and S. Ihl Woo, *Catal. Rev.: Sci. Eng.*, 2006, **48**, 43–89.
- 10 H. Jiang, Q. Wang, H. Wang, Y. Chen and M. Zhang, *ACS Appl. Mater. Interfaces*, 2016, **8**, 26817–26826.
- 11 T. Boningari, D. K. Pappas, P. R. Ettireddy, A. Kotrba and P. G. Smirniotis, *Ind. Eng. Chem. Res.*, 2015, **54**, 2261–2273.
- 12 J. Xu, H. Li, Y. Liu, L. Huang, J. Zhang, L. Shi and D. Zhang, *RSC Adv.*, 2017, **7**, 36319–36325.
- 13 L. Yan, Y. Liu, K. Zha, H. Li, L. Shi and D. Zhang, *ACS Appl. Mater. Interfaces*, 2017, **9**, 2581–2593.
- 14 Y. Li, Y. Wan, Y. Li, S. Zhan, Q. Guan and Y. Tian, *ACS Appl. Mater. Interfaces*, 2016, **8**, 5224–5233.
- 15 H. Y. Huang and R. T. Yang, *Langmuir*, 2001, **17**, 4997–5003.
- 16 C. Liu, G. Gao, J.-W. Shi, C. He, G. Li, N. Bai and C. Niu, *Chem. Commun.*, 2016, **86**, 36–40.
- 17 L. Chen, Z. Si, X. Wu and D. Weng, *ACS Appl. Mater. Interfaces*, 2014, **6**, 8134–8145.
- 18 K. Cheng, J. Liu, T. Zhang, J. Li, Z. Zhao, Y. Wei, G. Jiang and A. Duan, *J. Environ. Sci.*, 2014, **26**, 2106–2113.
- 19 B. Shen, T. Liu, N. Zhao, X. Yang and L. Deng, *J. Environ. Sci.*, 2010, **22**, 1447–1454.
- 20 D. K. Pappas, T. Boningari, P. Boolchand and P. G. Smirniotis, *J. Catal.*, 2016, **334**, 1–13.
- 21 P. R. Ettireddy, N. Ettireddy, T. Boningari, R. Pardemann and P. G. Smirniotis, *J. Catal.*, 2012, **292**, 53–63.
- 22 L. Zhang, S. Cui, H. Guo, X. Ma and X. Luo, *J. Mol. Catal. A: Chem.*, 2014, **390**, 14–21.
- 23 T. H. Vuong, J. Radnik, J. Rabeah, U. Bentrup, M. Schneider, H. Atia, U. Armbruster, W. Grünert and A. Brückner, *ACS Catal.*, 2017, **7**, 1693–1705.
- 24 F. Cao, S. Su, J. Xiang, P. Wang, S. Hu, L. Sun and A. Zhang, *Fuel*, 2015, **139**, 232–239.
- 25 Y. Wang, X. Li, L. Zhan, C. Li, W. Qiao and L. Ling, *Ind. Eng. Chem. Res.*, 2015, **54**, 2274–2278.
- 26 G. Qi, R. T. Yang and R. Chang, *Appl. Catal., B*, 2004, **51**, 93–106.
- 27 S. M. Lee, K. H. Park and S. C. Hong, *Chem. Eng. J.*, 2012, **195**, 323–331.
- 28 B. Shen, X. Zhang, H. Ma, Y. Yao and T. Liu, *J. Environ. Sci.*, 2013, **25**, 791–800.
- 29 B. Izadkhah, A. Niaei, M. J. Illán-Gómez, D. Salari, A. Tarjomannejad and V. Albaladejo-Fuentes, *Ind. Eng. Chem. Res.*, 2017, **56**, 3880–3886.
- 30 H. Jiang, J. Zhou, C. Wang, Y. Li, Y. Chen and M. Zhang, *Ind. Eng. Chem. Res.*, 2017, **56**, 3542–3550.
- 31 B. Thirupathi and P. G. Smirniotis, *Appl. Catal., B*, 2011, **110**, 195–206.
- 32 J. Liu, L. Yu, Z. Zhao, Y. Chen, P. Zhu, C. Wang, Y. Luo, C. Xu, A. Duan and G. Jiang, *J. Catal.*, 2012, **285**, 134–144.
- 33 M. Koebel, G. Madia, F. Raimondi and A. Wokaun, *J. Catal.*, 2002, **209**, 159–165.
- 34 A. Khan and P. G. Smirniotis, *J. Mol. Catal. A: Chem.*, 2008, **280**, 43–51.
- 35 T. Zhang, J. Liu, D. Wang, Z. Zhao, Y. Wei, K. Cheng, G. Jiang and A. Duan, *Appl. Catal., B*, 2014, **148**, 520–531.
- 36 L. Xu, X.-S. Li, M. Crocker, Z.-S. Zhang, A.-M. Zhu and C. Shi, *J. Mol. Catal. A: Chem.*, 2013, **378**, 82–90.
- 37 M. Koebel, M. Elsener and G. Madia, *Ind. Eng. Chem. Res.*, 2001, **40**, 52–59.
- 38 G. K. Reddy, J. He, S. W. Thiel, N. G. Pinto and P. G. Smirniotis, *J. Phys. Chem. C*, 2015, **119**, 8634–8644.
- 39 B. Thirupathi and P. G. Smirniotis, *J. Catal.*, 2012, **288**, 74–83.
- 40 B. M. Reddy, K. N. Rao, G. K. Reddy and P. Bharali, *J. Mol. Catal. A: Chem.*, 2006, **253**, 44–51.
- 41 G. Qi and W. Li, *Catal. Today*, 2015, **258**, 205–213.

